ChemComm

COMMUNICATION

View Article Online
View Journal | View Issue

Cite this: *Chem. Commun.*, 2019, 55, 12200

Received 24th July 2019,
Accepted 10th September 2019

DOI: 10.1039/c9cc05727g

rsc.li/chemcomm

Two-dimensional supramolecular assemblies based on β-cyclodextrin-grafted graphene oxide for mitochondrial dysfunction and photothermal therapy†

Bing Zhang,[ab] Qilin Yu,[c] Ying-Ming Zhang[a] and Yu Liu*[ab]

β-Cyclodextrin (CD)-grafted graphene oxide (GO) is an emerging drug carrier for human diseases therapy. Herein, we report two-dimensional nano-supramolecular assemblies to specifically target and disrupt tumor cell mitochondria in a photocontrollable manner. Moreover, the nanoassemblies displayed extremely high near-infrared-induced photothermal efficiency.

Mitochondrial dysfunction is one of the most important players in human diseases, including cancers, diabetes, obesity, immune disorders, and neurodegenerative diseases.[1–3] In particular, excessive mitochondrion metabolism plays an essential role in tumor growth and metastasis.[4,5] Therefore, the use of therapies that disrupt mitochondrial function in tumor cells is an emerging anticancer strategy. Both abnormal mitochondrial distribution and electron transfer disorder from itself would lead to serious cellular discordance reflected in cell cycle arrest, ATP level decrease and even cell death.[6,7] However, mitochondrion-based therapies are commonly compromised by poor mitochondrion-targeting ability.[8–11] Therefore, the development of dual-function agents (*i.e.*, agents that both target mitochondria and disrupt their function) is a promising strategy for improving the efficacy of mitochondrion-based therapies.

Supramolecular nanoassemblies show promise for this purpose.[12–14] Supramolecular nanoassemblies held together by noncovalent interactions have considerable potential for biomedical applications in general, owing to their ability to respond dynamically and reversibly to stimuli such as light, pH, oxygen, heat, and magnetism.[15,16] Various types of nanoassemblies—mainly nanoparticles (zero-dimensional) and nanofibers (one-dimensional)—have been constructed for the delivery of drugs and genes,[17–19] and several targeting nanoassemblies designed to improve the efficacy of photodynamic anticancer therapies were recently reported.[20,21] The development of dual-function, multistimuli-responsive supramolecular nanoassemblies that could both actively target and efficiently disrupt mitochondrial function would be highly desirable.

In this study, we designed and prepared two-dimensional (2D) host–guest supramolecular nanoassemblies based on a host consisting of β-cyclodextrin (CD)-grafted graphene oxide (GOCD) and a guest (designated TPM-Azo) consisting of transferrin (TF, a tumor-targeting protein) modified with polylysine (Plys, a polymer with multiple modification sites), mitochondrion-targeting peptide (MitP), azobenzene (Azo), and polyethylene glycol (PEG) (Scheme 1). These nanoassemblies, designated TPM-Azo⊂GOCD, specifically targeted the mitochondria of tumor cells, reversibly responded to ultraviolet-visible (UV-vis) irradiation, and severely disrupted mitochondrial function, leading to remarkable inhibition of tumor growth both by cell cycle arrest and by near-infrared-light (NIR)-induced cell death.

To prepare TPM-Azo, the guest component of the nanoassemblies, we covalently modified TF with polylysine, polyethylene glycol (PEG-NH_2), MitP, and the photoactive molecule 4-(phenylazo)benzoic acid (Azo-COOH) in a two-step reaction mediated by EDC/NHSS (Scheme 1). The Azo and PEG moieties endowed TPM-Azo with binding affinity for β-CD and good stability in water and biological milieu. SDS-PAGE analysis revealed that TPM-Azo had a molecular weight of 75–80 kD, which is slightly higher than that of TF (70 kD) (Fig. 1a). FT-IR spectroscopy indicated the presence of PEG and $-NH_2$ groups in TPM-Azo (Fig. S1, ESI†). TPM-Azo, which was a mixture of *cis* and *trans* isomers, was irradiated with visible light (520 nm) to thoroughly produce TPM-*trans*-Azo, which can form complexes with β-CD (Fig. S2, ESI†).

To obtain the GOCD precursor, we first prepared large sheets of graphene oxide by the modified Hummers' method.[22] These sheets then received high-intensity sonication in distilled water to

[a] *College of Chemistry, State Key Laboratory of Elemento-Organic Chemistry, Nankai University, Tianjin 300071, China*
[b] *Collaborative Innovation Center of Chemical Science and Engineering (Tianjin), Tianjin 300072, China*
[c] *Key Laboratory of Molecular Microbiology and Technology, Ministry of Education, College of Life Sciences, Nankai University, Tianjin 300071, China*

† Electronic supplementary information (ESI) available: Detailed synthesis, characterization data, mitochondrial aggregation analysis, ATP levels, cell viability, the release of cytochrome *c*. See DOI: 10.1039/c9cc05727g

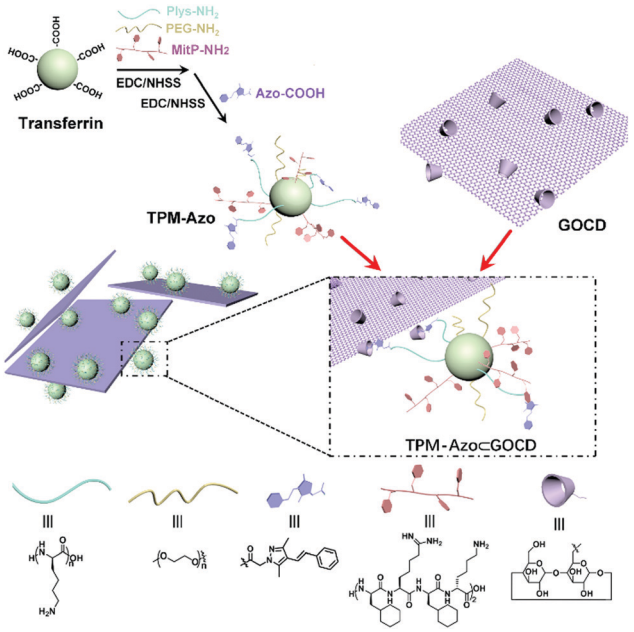

Scheme 1 Synthesis of the TPM-Azo guest, the GOCD host, and the TPM-Azo⊂GOCD host–guest supramolecular nanoassemblies.

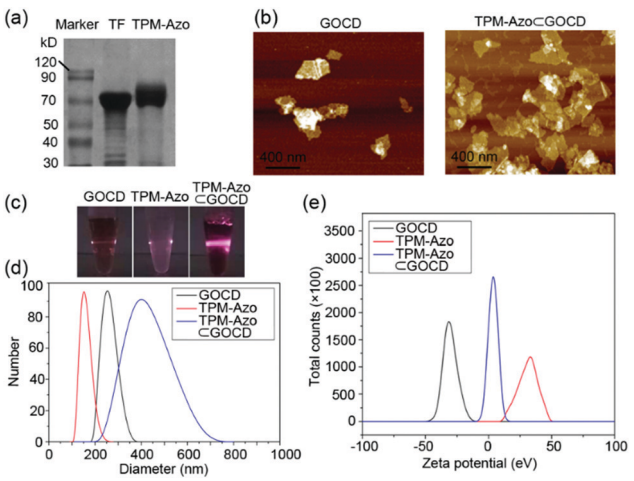

Fig. 1 Characterization of TPM-Azo, GOCD, and the TPM-Azo⊂GOCD supramolecular nanoassemblies. (a) SDS-PAGE analysis of TF and TPM-Azo. (b) Atomic force microscopy images of GOCD and TPM-Azo⊂GOCD. (c) Tyndall images of GOCD, TPM-Azo, and TPM-Azo⊂GOCD. (d) Dynamic light scattering data for GOCD (50 mg L^{-1}), TPM-Azo (50 mg L^{-1}), and TPM-Azo⊂GOCD ([GOCD] = [TPM-Azo] = 50 mg L^{-1}). (e) Zeta potentials of GOCD, TPM-Azo, and TPM-Azo⊂GOCD.

generate small-size GO (sGO) with sizes of 50–200 nm, thicknesses of 1–2 nm (Fig. S3, ESI†), and –COOH groups on the surface (as indicated by FT-IR). The sGO was derivatized with mono-6-deoxyl-6-ethylenediamino-CD by means of an EDC/NHSS-mediated reaction to obtain the GOCD,[23] which served as the host component of the 2D supramolecular nanoassemblies. Atomic force microscopy showed that the size and thickness of the GOCD were comparable to those of the sGO (Fig. 1b and Fig. S3, ESI†). FT-IR analysis revealed the presence of –CO–NH– and –OH groups on the GOCD (Fig. S4, ESI†).

As expected, when equal concentrations of GOCD and TPM-Azo were mixed, 2D TPM-Azo⊂GOCD aggregates with sizes of 400–800 nm and thicknesses of 2–4 nm formed (Fig. 1b). Unlike GOCD and TPM-Azo, the TPM-Azo⊂GOCD aggregates showed an obvious Tyndall effect (Fig. 1c). Dynamic light scattering analysis indicated that the sizes of the TPM-Azo⊂GOCD aggregates ranged from 200 to 750 nm, with an average size of 420 nm, which is approximately twice the average sizes of GOCD (150 nm) and TPM-Azo (280 nm) (Fig. 1d). Zeta potential analysis revealed that the aggregates had a weakly positive zeta potential (with a peak potential of +5), whereas GOCD had a negative zeta potential (–30) and TPM-Azo had a positive one (+35) (Fig. 1e). These observations confirm that GOCD and TPM-Azo combined to form 2D TPM-Azo⊂GOCD supramolecular nanoassemblies.

Because of the MitP on the surface of the TPM-Azo guest, it can be expected to bind mitochondria, and furthermore, the presence of GOCD on the host might induce mitochondrial aggregation during formation of the 2D nanoassemblies (Fig. 2a). In fact, when fluorescein-isothiocyanate-tagged TPM-Azo was incubated with 4′,6-diamidino-2-phenylindole-labelled mitochondria which were isolated from A549 tumor cells, the fluorescence of TPM-Azo overlapped perfectly with the fluorescence of the mitochondria, indicating that TPM-Azo efficiently bound the mitochondria (Fig. 2b). Moreover, remarkable mitochondrial aggregation was induced by subsequent addition of GOCD, as indicated by the observation of abundant mitochondrial aggregates overlapping with the fluorescence of the TPM-Azo⊂GOCD nanoassemblies in fluorescence microscopy images (Fig. 2b, white arrows). Notably, GOCD alone did not cause mitochondrial aggregation, and in addition, UV-irradiation-induced transformation of TPM-*trans*-Azo to TPM-*cis*-Azo led to partial disassembly of the mitochondrial aggregates (Fig. S5, ESI†). These results confirm that formation of the TPM-Azo⊂GOCD nanoassemblies efficiently induced mitochondrial aggregation *in vitro*.

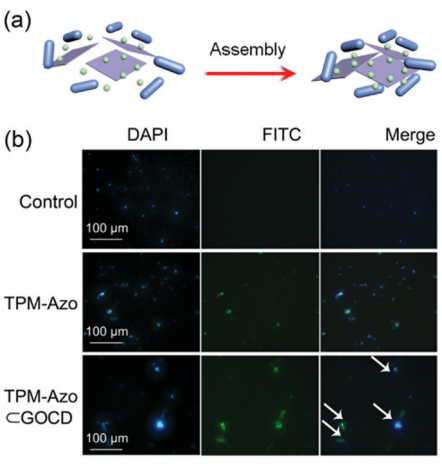

Fig. 2 Mitochondrial aggregation induced by the TPM-Azo⊂GOCD nanoassemblies. (a) Schematic illustration of mitochondrial aggregation mediated by the combination of fluorescein-isothiocyanate-tagged TPM-Azo and GOCD. (b) Fluorescence microscopy images showing mitochondrial aggregation (white arrows) induced by TPM-Azo⊂GOCD but not by TPM-Azo.

After co-incubation of fluorescein-isothiocyanate-tagged TPM-Azo or the TPM-Azo⊂GOCD nanoassemblies with MitoTracker-Red-stained A549 cells, the fluorescence of fluorescein isothiocyanate overlapped with the fluorescence of MitoTracker Red, indicating that the guest and the nanoassemblies could target the tumor mitochondria (Fig. 3). In addition, GOCD and TPM-Azo alone had no impact on the morphology of the mitochondrial network (Fig. 3 and Fig. S6, ESI†), whereas treatment with the nanoassemblies led to remarkable mitochondrial aggregation (Fig. 3, indicated by the white arrow in the panels labelled Control panels). Moreover, irradiation with visible light (520 nm) exacerbated this aggregation (Fig. 3, white arrows in the Vis panels), whereas UV irradiation (365 nm) attenuated the effect of the nanoassemblies (Fig. 3, UV panels). Consistent with these results, ATP assays revealed that intracellular ATP levels were decreased by the nanoassemblies, and the decrease was larger upon visible-light irradiation and smaller upon UV irradiation (Fig. S7, ESI†). Together, these results suggest that the photocontrollable formation of the TPM-Azo⊂GOCD nanoassemblies may have led to mitochondrial aggregation followed by mitochondrial disruption.

Because mitochondria are the key generators of energy in cells, mitochondrial dysfunction can be expected to severely disrupt the progression of the cell cycle.[24] Therefore, we performed a flow-cytometry-based cell cycle assay to evaluate the effect of the nanoassemblies on the cell cycle in A549 tumor cells. As expected, when the assay was carried out in the dark (no irradiation), the TPM-Azo⊂GOCD nanoassemblies increased the percentage of G2-phase cells (from 21.4% to 23.3%) and decreased the percentage of S-phase cells (from 18.6% to 16.9%) (Fig. S8a and b, ESI†), implying that the nanoassemblies induced cell cycle arrest at the G2 phase. More strikingly, visible-light irradiation enhanced the deleterious effect of the nanoassemblies, increasing the percentage of G2-phase cells to 32.8% (Fig. S8c, ESI†), whereas the effect of UV irradiation was less pronounced (Fig. S8d, ESI†).

In addition, a cell counting kit assay showed that under visible-light irradiation, the TPM-Azo⊂GOCD nanoassemblies clearly decreased cell viability (from 100% to 78%) (Fig. 4a and Fig. S9, ESI†), whereas no obvious effect on viability was observed under UV irradiation (Fig. S9, ESI†). These findings suggest that the TPM-Azo⊂GOCD nanoassemblies caused photocontrollable cell cycle arrest and a decrease in cell viability.

Owing to the potential of activity under NIR irradiation,[25] we hypothesized that the nanoassemblies might be useful for photothermal therapy. In fact, heat mapping revealed that like GOCD, TPM-Azo⊂GOCD nanoassemblies that had been irradiated with visible light increased the temperature of the nanoassembly solution from 20 to 65 °C in 5 min upon exposure to NIR light (808 nm, 1.5 W) (Fig. S10, ESI†), indicating that the nanoassemblies had good photothermal transition activity.

We then investigated the effects of visible-light-irradiated TPM-Azo⊂GOCD nanoassemblies on A549 tumor cells upon exposure to NIR irradiation. Both GOCD and the TPM-Azo⊂GOCD nanoassemblies significantly decreased cell viability, whereas TPM-Azo did not (Fig. 4a). Interestingly, the decrease in cell viability induced by treatment with the nanoassemblies (81%) was much larger than that observed upon treatment with GOCD (55%). Western blotting revealed that under NIR irradiation, treatment with the nanoassemblies caused much higher levels of cytochrome *c* release from the mitochondria to the cytoplasm than did treatment

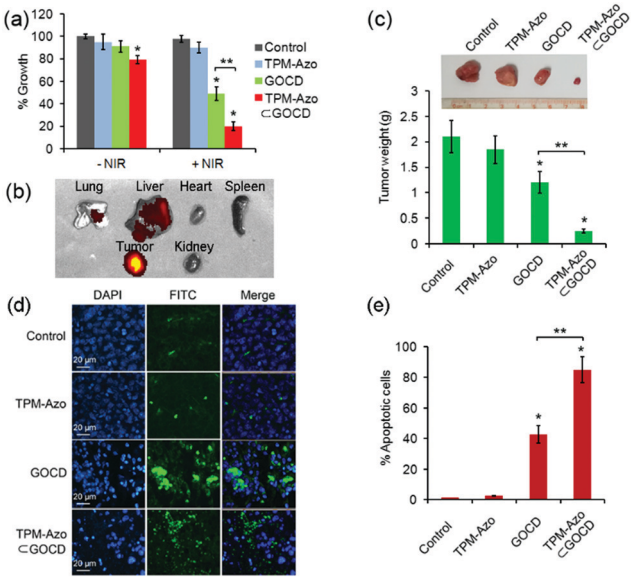

Fig. 4 Antitumor activities of the nanoassemblies. (a) *In vitro* antitumor cell activities of TPM-Azo (100 mg L^{-1}), GOCD (100 mg L^{-1}), and TPM-Azo⊂GOCD assemblies ([TPM-Azo] = [GOCD] = 100 mg L^{-1}) in A549 tumor cells in the absence or presence of NIR irradiation (−NIR and +NIR, respectively). (b) *In vivo* distribution of the nanoassemblies in various organs 24 hours after intravenous injection into S180-tumor-bearing mice. (c) Images of tumors and weights of tumors after treatment of S180-tumor-bearing mice with NIR irradiation (808 nm, 1.5 W) and TPM-Azo (100 mg kg^{-1}), GOCD (100 mg kg^{-1}), or TPM-Azo⊂GOCD (100 mg kg^{-1} of TPM-Azo and 100 mg kg^{-1} GOCD). (d) TUNEL images of tumor tissues after treatment with the nanoassemblies and NIR irradiation. (e) Percentages of TUNEL-positive (apoptotic) cells in the tumor tissues. * indicates a significant difference between the control group and the treated group ($P < 0.05$); ** indicates a significant difference between the GOCD group and the TPM-Azo⊂GOCD group ($P < 0.01$).

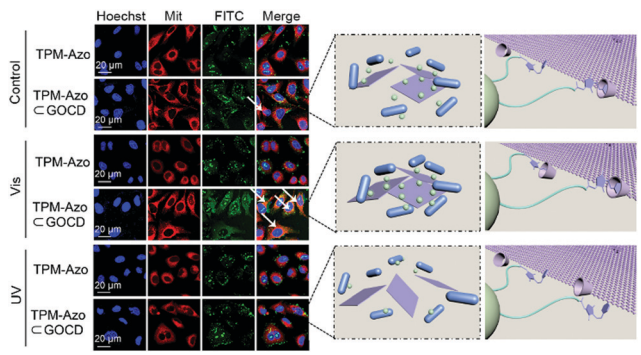

Fig. 3 Light-controlled intracellular mitochondrial disruption by TPM-Azo⊂GOCD. TPM-Azo⊂GOCD induced mitochondrial disruption (white arrows) after visible-light irradiation (Vis, 520 nm) but not after UV irradiation (UV, 365 nm). The effect of TPM-Azo⊂GOCD on intracellular mitochondrial dynamics was investigated by confocal microscopy.

with GOCD or TPM-Azo alone (Fig. S11, ESI†), indicating that under these conditions, the nanoassemblies may have damaged the mitochondria more severely than did either the host or the guest. However, the TPM-Azo⊂GOCD nanoassemblies had little effect on the viability of normal NIH3T3 cells, even with NIR treatment (Fig. S12, ESI†), indicating that the nanoassemblies were essentially nontoxic to normal cells. Therefore, the combining of mitochondrial aggregation and NIR toxicity of TPM-Azo⊂GOCD nanoassemblies successfully enhanced the killing efficiency for the tumor cell.

The *in vivo* antitumor activity of the nanoassemblies was also evaluated in S180-tumor-bearing mice.[11,26] Fluorescence imaging revealed that nanoassemblies accumulated mainly in the primary tumor but could also be found in the lung and the liver 24 h after injection (Fig. 4b), indicating that the nanoassemblies had good tumor-targeting ability. Twelve days after treatment of the mice with NIR irradiation in combination with the nanoassemblies, TPM-Azo, or GOCD, the nanoassemblies showed stronger antitumor activity than TPM-Azo or GOCD alone, decreasing tumor weight to approximately 10% of the original weight (Fig. 4c). In addition, a TdT-mediated dUTP nick-end labeling (TUNEL) assay indicated that the nanoassemblies killed 80% of the tumor cells in the tumor tissues, whereas TPM-Azo or GOCD alone killed $<50\%$ of the cells (Fig. 4d and e). Taken together, these results show that the nanoassemblies had strong antitumor activity both *in vitro* and *in vivo* when used in combination with NIR irradiation.

In summary, we constructed 2D host–guest supramolecular nanoassemblies composed of GOCD as the host and a tumor-targeting protein modified with a peptide and azobenzene as the guest (TPM-Azo). These nanoassemblies specifically targeted the mitochondria of tumor cells and severely disrupted mitochondrial function in a photocontrollable manner, leading to remarkable inhibition of tumor growth as a result of both cell cycle arrest and NIR-induced cell death. The use of such supramolecular nanoassemblies for photothermal therapy aimed at inducing mitochondrial dysfunction represents an exciting, novel strategy for cancer therapy.

We are thankful to the National Natural Science Foundation of China (21432004, 31870139, 21472100, 21772099, and 91527301) and the China Postdoctoral Science Foundation (2018M641632).

Conflicts of interest

There are no conflicts to declare.

Notes and references

1 S. Selvaraji, L. Poh, V. Natarajan, K. Mallilankaraman and T. V. Arumugam, *Cond. Med.*, 2019, **2**, 30–39.
2 H. J. Kwon, M. Y. Cha, D. Kim, D. K. Kim, M. Soh, K. Shin, T. Hyeon and I. Mook-Jung, *ACS Nano*, 2016, **10**, 2860–2870.
3 M. T. Lin and M. F. Beal, *Nature*, 2006, **443**, 787–795.
4 A. R. Choudhury and K. K. Singh, *Semin. Cancer Biol.*, 2017, **47**, 125–146.
5 M. E. Lleonart, R. Grodzicki, D. M. Graifer and A. Lyakhovich, *Med. Res. Rev.*, 2017, **37**, 1275–1298.
6 L. H. Xu, G. H. Tong, Q. L. Song, C. Y. Zhu, H. L. Zhang, J. J. Shi and Z. Z. Zhang, *ACS Nano*, 2018, **12**, 6806–6818.
7 G. Pandey, N. Mittapelly, V. T. Banala and P. R. Mishra, *ACS Appl. Mater. Interfaces*, 2018, **10**, 16964–16976.
8 K. A. Sarosiek and A. Letai, *FEBS J.*, 2016, **283**, 3523–3533.
9 Z. P. Chen, M. Li, L. J. Zhang, J. Y. He, L. Wu, Y. Y. Xiao, J. A. Duan, T. Cai and W. D. Li, *J. Drug Targeting*, 2016, **24**, 492–502.
10 W. Lv, Z. Zhang, K. Y. Zhang, H. Yang, S. Liu, A. Xu, S. Guo, Q. Zhao and W. Huang, *Angew. Chem., Int. Ed.*, 2016, **55**, 9947–9951.
11 Q. Yu, Y. M. Zhang, Y. H. Liu, X. Xu and Y. Liu, *Sci. Adv.*, 2018, **44**, eaat2297.
12 L. L. Rui, Y. D. Xue, Y. Wang, Y. Gao and W. A. Zhang, *Chem. Commun.*, 2017, **53**, 3126–3129.
13 A. P. Thomas, L. Palanikumar, M. T. Jeena, K. Kim and J. H. Ryu, *Chem. Sci.*, 2017, **8**, 8351–8356.
14 Y. T. Shen, L. J. Liang, S. Q. Zhang, D. S. Huang, R. Deng, J. Zhang, H. X. Qu, S. P. Xu, C. Y. Liang and W. Q. Xu, *ACS Appl. Mater. Interfaces*, 2018, **10**, 7910–7918.
15 Y. M. Zhang, N. Y. Zhang, K. Xiao, Q. Yu and Y. Liu, *Angew. Chem., Int. Ed.*, 2018, **57**, 8649–8653.
16 J. Zhuang, H. Secinti, B. Zhao and S. Thayumanavan, *Angew. Chem., Int. Ed.*, 2018, **57**, 7111–7115.
17 Y. Kang, K. Guo, B. J. Li and S. Zhang, *Chem. Commun.*, 2014, **50**, 11083–11092.
18 R. Dong, Y. Zhou, X. Huang, X. Zhu, Y. Lu and J. Shen, *Adv. Mater.*, 2015, **27**, 498–526.
19 X. Ma and Y. Zhao, *Chem. Rev.*, 2015, **115**, 7794–7839.
20 X. W. Hua, Y. W. Bao, J. Zeng and F. G. Wu, *ACS Appl. Mater. Interfaces*, 2018, **10**, 42077–42087.
21 C. Yue, Y. Yang, J. Song, G. Alfranca, C. Zhang, Q. Zhang, T. Yin, F. Pan, J. M. de la Fuente and D. Cui, *Nanoscale*, 2017, **9**, 11103–11118.
22 J. P. Liu, Y. Chen, G. Y. Li, P. Y. Zhang, C. Z. Jin, L. L. Zeng, L. N. Ji and H. Chao, *Biomaterials*, 2015, **56**, 140–153.
23 F. W. Low, C. W. Lai and S. B. Abd Hamid, *J. Nanosci. Nanotechnol.*, 2015, **15**, 6769–6773.
24 Y. M. Zhang, Y. Cao, Y. Yang, J. T. Chen and Y. Liu, *Chem. Commun.*, 2014, **50**, 13066–13069.
25 L. Y. Yang, Y. T. Tseng, G. L. Suo, L. L. Chen, J. T. Yu, W. J. Chiu, C. C. Huang and C. H. Lin, *ACS Appl. Mater. Interfaces*, 2015, **7**, 5097–5106.
26 Q. J. He, D. O. Kiesewetter, Y. Qu, X. Fu, J. Fan, P. Huang, Y. J. Liu, G. Z. Zhu, Y. Liu, Z. Y. Qian and X. Y. Chen, *Adv. Mater.*, 2015, **27**, 6741–6746.